Available online at www.sciencedirect.com
SCIENCE DIRECT®
Surface Science 552 (2004) 85–97
SURFACE SCIENCE
www.elsevier.com/locate/susc

Formation of a faceted MoO_2 epilayer on Mo(1 1 2) studied by XPS, UPS and STM

T. Schroeder [a,*], J. Zegenhagen [a], N. Magg [b], B. Immaraporn [b], H.-J. Freund [b]

[a] E.S.R.F., ID 32, 6, Rue Jules Horowitz, 38043 Grenoble, France
[b] Fritz-Haber-Institut der Max-Planck-Gesellschaft, Faradayweg 4-6, 14195 Berlin, Germany

Received 26 November 2003; accepted for publication 13 January 2004

Abstract

The open trough and row Mo(1 1 2) surface serves as substrate for the epitaxial growth of MoO_2. XPS, UPS and STM studies of the oxygen adsorption allow to monitor step-by-step the transformation of the electronic and morphological properties during this process. XPS and UPS spectra reveal that a stable oxygen chemisorbed state precedes the formation of MoO_2. STM topographs identify this oxygen chemisorbed phase as an oxygen-induced $p(2\times3)$ reconstruction of the missing row type. This precursor state evolves into a flat $p(1\times3)$ reconstructed (0 1 0) MoO_2 layer which roughens by the formation of (1 1 0) facets under further oxygen exposure.

Keywords: X-ray photoelectron spectroscopy; Visible and ultraviolet photoelectron spectroscopy; Scanning tunneling microscopy; Surface relaxation and reconstruction; Chemisorption; Oxidation; Epitaxy; Faceting

1. Introduction

Experimentally and theoretically, the Mo(1 1 2) surface was studied in very different aspects. In earlier works, the corrugation of the furrowed Mo(1 1 2) surface has been exploited to study the interaction of chemisorbed particles [1–4]. The role of the electronic structure of the highly anisotropic substrate has been found to be decisive to explain the detected adsorbate structures. Therefore, the band structure of the Mo(1 1 2) surface has been studied by self-consistent electronic structure calculations [5] as well as by angle-resolved photoemission spectroscopy (ARPES) [6–9]. Furthermore, the (1 1 2) surface of refractive Mo is currently used as substrate for the epitaxial growth of thin magnetic gadolinium films (metal-on-metal epitaxy) [10,11] as well as for ultra-thin crystalline silica epilayers (insulator-on-metal epitaxy) [12–14]. The latter studies had been performed by the authors of the present paper in the field of model catalysis and had motivated us to carry out the first extensive analysis of the oxidation behaviour of the Mo(1 1 2) surface. Oxygen-induced structures as well as oxides on the stable low index (1 0 0), (1 1 0) and (1 1 1) surfaces of Mo have been widely used in the past to unravel structure–reactivity relationships of molybdenum oxide based catalysts [15–20]. In case of Mo(1 1 2), only oxygen adsorption studies at low coverages have been reported in the literature [21–23], but no systematic

* Corresponding author. Tel.: +33-4-76882722; fax: +33-4-76882325.
E-mail address: thomas.schroeder@esrf.fr (T. Schroeder).

0039-6028/$ - see front matter © 2004 Elsevier B.V. All rights reserved.
doi:10.1016/j.susc.2004.01.010

work on its oxidation behaviour of the Mo(1 1 2) surface, as detailed as those on the other low-index Mo surfaces, has been published so far. A recent study exploited an oxygen-induced p(1×3) reconstruction and thin MoO_2 layers on Mo(1 1 2) to study the growth behaviour of Ag clusters on these supports, but did not address the changes in the electronic and morphological properties of the resulting surface phases during the oxidation process [24]. Therefore, in the present work, the step-by-step transformation of the properties of the clean Mo(1 1 2) surface under oxygen exposure into an epitaxially grown MoO_2 film has been monitored, applying X-ray/ultraviolet photoemission spectroscopy (XPS/UPS) for electronic and scanning tunneling microscopy (STM) for surface crystallographic structure analysis. As outlined in detail in a previous publication [25], an oxygen-induced p(2×3) reconstruction has been found to precede the MoO_2 formation on the Mo(1 1 2) surface. In this paper, the morphological studies will focus on the processes involved in transforming this oxygen-induced precursor state into an epitaxial MoO_2 layer.

2. Experimental

The experiments were carried out in a multichamber UHV system with an integrated in situ sample transfer system and a base pressure of 2×10^{-10} mbar [26]. The main chamber includes an hemispherical energy analyzer (Scienta SES-200) with non-monochromized Mg-K_α (1253.6 eV) and He I (21.21 eV) radiation sources for XPS and UPS studies, respectively. Binding energies reported in this paper are referenced to the Fermi level of the Mo substrate and spectra were recorded under normal emission. These studies are supplemented by measurements in the STM chamber yielding real space images obtained in the constant current mode at room temperature. Reported biases are referenced with respect to the sample. The preparation chambers are equipped with thermocouples (type C as well as type K) and a gas doser system to conduct the following oxidation study with control of temperature and gas pressure. The cleaning procedure of the Mo(1 1 2) surface has been carried out in the high temperature chamber as described in the literature [27]. Oxidation at 1500 K was followed by several high temperature flashes to approximately 2300 K to desorb any molybdenum oxides from the surface. Spectra and images of the clean Mo(1 1 2) surface presented in the following are labeled with the number (0). The transformation of the clean Mo(1 1 2) surface into an epitaxial MoO_2 layer was monitored in the main chamber by studying the oxidation behaviour in 13 discrete oxidation steps (1–13). In each step the crystal surface was exposed to 5×10^{-6} mbar oxygen (O_2) for 6 min (1.8×10^3 L) after the crystal had reached its oxidation temperature. In order to produce MoO_2 layers of different thickness, three temperature regimes were applied and steps (1–8), (9–12) and (13) were carried out at 950, 1100 and 1250 K, respectively. Note that after each of the oxidation steps, the crystal was annealed by heating it in UHV (without oxygen!) to 1300 K for 15 min. No change in the amount of adsorbed oxygen occurs during these annealing steps, as controlled by XPS. Spectra and images taken during the oxidation procedure (1–13) were always measured after the corresponding annealing step and were denoted accordingly by the numbers (1)–(13).

3. Results and discussion

3.1. XPS study of the chemical composition

The results of the XPS study on the transformation of the Mo(1 1 2) surface into an epitaxial MoO_2 layer are summarized in Fig. 1 with the left and the right panel showing the analysis of the Mo_{3d} and the O_{1s} signals, respectively.

The Mo_{3d} photoelectron spectrum of the clean Mo(1 1 2) surface (0) exhibits a strong spin–orbit splitting with the Mo $3d_{5/2}$ line situated at 227.7 eV and the Mo $3d_{3/2}$ component at 231 eV. Where the corresponding O_{1s} signal would be located, only a very small signal can be distinguished (0). As pointed out in the STM study below, this rest signal is probably due to some oxygen contamination of the surface region remaining from the high temperature oxidation step of the crystal cleaning procedure.

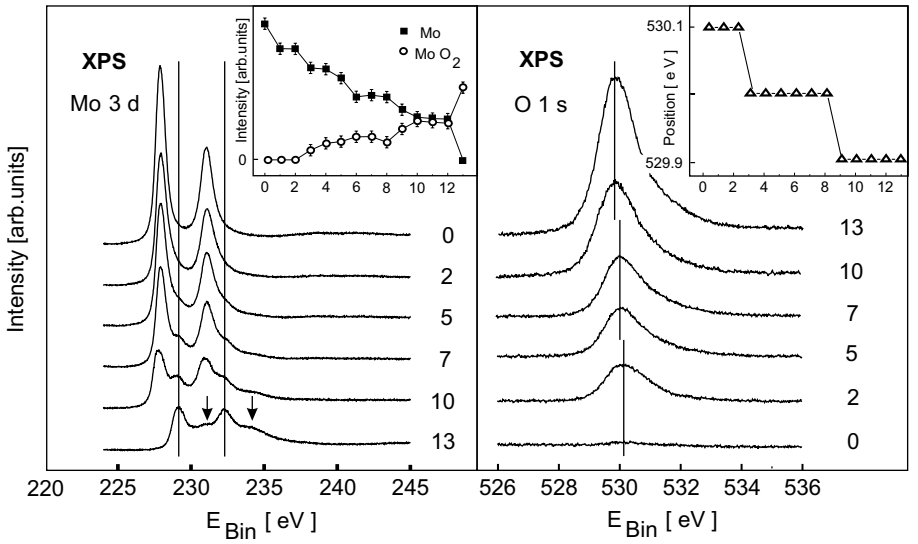

Fig. 1. Step-by-step XPS study of the Mo_{3d} (left panel) and the O_{1s} (right panel) photoelectron lines during the transformation process of the clean Mo(1 1 2) surface into MoO_2 under progressive oxygen exposure (0–13). Inset on the left shows the intensity of metallic (Mo) and oxidic (MoO_2) components in the Mo_{3d} spectra, the inset on the right summarizes the position of O_{1s} lines.

The oxygen-induced p(2×3) surface reconstruction on the Mo(1 1 2) substrate fully evolves after the application of the first oxidation step and, with the oxidation parameters chosen here, remains stable under oxidation step (2) [25]. It is important to note that the corresponding Mo_{3d} photoelectron spectrum (2) shows only metallic line components without any detectable traces of oxide peaks. Therefore, oxygen chemisorption and not oxidation induces the p(2×3) surface reconstruction. Certainly, the oxygen chemisorption process on the surface results in a decrease of the Mo_{3d} line intensity, as is depicted in the inset of the left panel. The well-evolved O_{1s} signal (2) allows to accurately derive a binding energy of 530.1 eV for oxygen chemisorbed on the Mo(1 1 2) surface (see inset in the right panel).

Further exposure to oxygen at 950 K during the steps (3)–(8) results in the oxidation of the Mo(1 1 2) surface. The onset of the oxidation is noticed in the Mo_{3d} photoelectron spectra by a small, but clearly detectable change in the shape of the two metallic spin–orbit components. To guide the eye, this region is marked in the left panel of Fig. 1 by two vertical lines. Comparison of the spectrum (2) (characteristic of the oxygen chemisorbed state) and the spectrum (5) (representative of the onset of the oxidation) reveals that the asymmetric shape of the metallic spin orbit components changes with progressing oxygen exposure from a rather exponential towards an almost linear form. Certainly, this is indicating the upcoming oxide peaks in the Mo_{3d} spectrum at these positions. After applying two additional oxidation steps, spectrum (7) clearly reveals that the Mo $3d_{5/2}$ and Mo $3d_{3/2}$ spin–orbit components of the oxide are situated at a binding energy of 229.25 and 232.4 eV, respectively. It is worthy of note that the preparation of molybdenum oxide on the Mo(1 1 2) surface produces in the corresponding O_{1s} signals (3–8) a small shift of 0.1 eV towards a binding energy of 530 eV. As can be inferred from the left inset in Fig. 1, the growth of the oxide saturates during the steps (4–8). According to the formalism described in the literature [28], the inelastic mean free path (IMFP) of Mo_{3d} photoelectrons excited by Mg-K_α radiation is calculated to be 24 Å. With this value, a saturation thickness of the oxide layer of 15 ± 1.5 Å results.

To grow a thicker MoO_2 layer, the oxygen pressure is kept constant, but the oxidation temperature is raised to 1100 K during the steps

(9–12). With these parameters, the oxide thickness saturates at about 28 ± 2.8 Å. This thicker oxide layer results in a strongly increased O_{1s} photoelectron intensity, as can be seen from the characteristic O_{1s} photoelectron line (10). In addition, the right inset shows that a further shift of 0.1 eV towards a lower binding energy value of 529.9 eV is detected for the O_{1s} signals (9–12). Interestingly, the increase of the oxide components in the Mo_{3d} photoelectron line (10) is accompanied by the appearance of a weak peak structure at 234.1 eV. As this points to a more complicated Mo_{3d} spectrum of the oxide, a reference spectrum (13) has been measured by increasing the oxidation temperature to 1250 K with all other oxidation parameters kept constant. While the O_{1s} spectrum (13) merely shows an intensity increase with no change in position, the shape of the Mo_{3d} spectrum changes dramatically. Due to the growth of an oxide thickness which substantially exceeds the Mo_{3d} IMFP value, no metallic components are visible in the spectrum (13). The oxide Mo_{3d} photoelectron spectrum can be distinguished and the reduction in the number of peaks simplifies its identification. The result of a fit procedure is that each of the spin–orbit components of the Mo_{3d} photoelectron line becomes split again with an intensity ratio of approximately 1:2. The line positions of the more intense oxide peaks are, as stated above, 229.25 eV for Mo $3d_{5/2}$ and 232.4 eV for Mo $3d_{3/2}$, resulting in a shift of 1.6 eV with respect to the metallic state. The positions of the less intense oxide signals are marked by arrows in Fig. 1 and are found to be 230.9 eV for Mo $3d_{5/2}$ and 234.1 eV for Mo $3d_{3/2}$ so that a shift of approximately 3.2 eV is detected with respect to the metallic state. As stated in the literature, these features are characteristic of the complex Mo_{3d} photoelectron line of MoO_2 which is strongly influenced by many particle effects [29,30].

3.2. UPS study of the valence band structure

Fig. 2 shows the result of the He I UPS study which traces the drastic changes in the valence band (VB) structure and work function (inset) during the transformation of the clean Mo(1 1 2) surface into a MoO_2 surface layer.

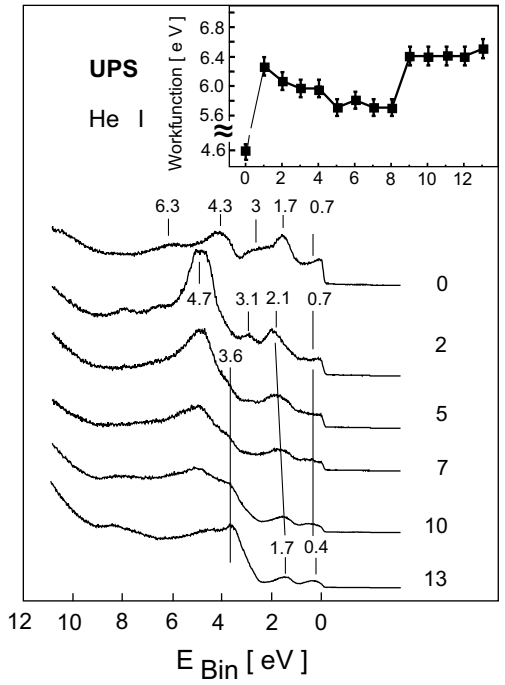

Fig. 2. Step-by-step He I UPS study of the valence band structure during the transformation process of the clean Mo(1 1 2) surface into MoO_2 under progressive oxygen exposure (0–13). The inset shows changes in the sample work function, as derived from the width of the UP spectra [54].

The Fermi level position of the He I UP spectrum (0) of the clean Mo(1 1 2) surface serves in the following as zero point for all given peak energies in the UP spectra. As Mo is a metal with partially filled 4d states, a peak in the photoemission intensity right at the Fermi level is indicating that the Fermi level crosses the d band. This region centered around −0.7 eV is followed by a strong peak at −1.7 eV. At higher binding energies, a broad shoulder around −3 eV is locked to that peak. The most intense feature in the clean Mo(1 1 2) spectrum is the peak at −4.3 eV and the last feature unambiguously resolved above the secondary electron background is a small peak at −6.3 eV. The He I spectrum reproduces well peak positions and intensity distribution found in earlier theoretical and experimental electronic structure studies on the Mo(1 1 2) surface [5–9]. One of these studies focussed on the interplay between the surface band structure and, based on the observed

Fermi level crossings, a scheme of possible electronically driven surface reconstructions was proposed [7]. It is interesting to note that the oxygen-induced p(2×3) reconstruction, discussed in the following, fits well into that scheme so that probably electronic structure aspects play an important role in the formation and stability of this adsorbate induced surface phase.

The He I UP spectrum (2) of the oxygen-induced p(2×3) surface reconstruction is dominated by the appearance of a strong peak at −4.7 eV. The next peak at lower binding energies is found at −3.1 eV and this peak is not stable under further oxygen exposure. In contrast to this, the intense peak at −2.1 eV increases in width and slightly shifts to smaller binding energies, but remains visible with progressing oxygen exposure. The structure, representative for the Mo(1 1 2) d band next to the Fermi level (peak region around −0.7 eV), remains stable during the whole oxygen exposure procedure, but substantially decreases in intensity. All these features of the electronic structure of the p(2×3) O–Mo(1 1 2) phase, together with the strong increase of the work function (inset in Fig. 2), fit well into the general framework of oxygen chemisorption on transition metals [31–33]. Oxygen–metal bond formation requires electron transfer from the Fermi level region of the metal valence band to the Mo–O bonding orbitals and this probably explains the detected intensity decrease at the Fermi level region. Furthermore, it is not surprising that a mere change in intensity, but no difference in fine structure is detected in the upper d valence band region next to the Fermi level. Wood et al. concluded that a characteristic feature of all d metals is that states in the upper part of the d band are more localized in real space than the states in the lower part of the d band [34]. Greater delocalization of d electrons at the bottom of the d band favours their hybridization with s-electrons which are known to be the most delocalized. This can be seen in the band structure of many transition metals where the main maximum of the partial density of s-states (s-PDOS) curve is located at the bottom of the d band. This is also the case for Mo, as can be seen in the PDOS curves of electronic structure calculations of bulk Mo [35,36]. The s-band main maximum coincides with the d band bottom part at around −4.5 eV [5] and makes only minor contribution to the total density of states in the upper d band region. Belash et al. have recently shown by monitoring the transformation of the electronic structure of Cu into Cu_2O through subsequent oxidation steps that for the formation of the oxygen–metal bonding band in the chemisorption process only those energy regions of the d band play a role for which the contribution from s-states becomes comparable to the contribution of d states [37]. This picture is supported by the results of our oxygen chemisorption study on the Mo(1 1 2) surface because the maximum of the bonding O–Mo peak, mainly O_{2p} in character and resulting from the interactions of O_{2p} electrons with Mo spd hybridized states, is found in our UP spectra at −4.7 eV which is in striking vicinity to the s-band maximum position at −4.5 eV.

Certainly, this oxygen chemisorption picture breaks down, as soon as the formation of a bulk MoO_2 phase starts due to strong oxygen incorporation into the Mo lattice. As this oxygen uptake results in a depolarization of the surface dipole of the reconstruction, a gradual work function decrease is indicative for this process [38]. The oxidation process on the Mo(1 1 2) surface, reported by XPS to start with the third oxidation step at 950 K, results indeed in such a gradual work function decrease for the VB spectra (3)–(8) and is depicted in the inset of Fig. 2. In addition, a general broadening of the peak structures and the disappearance of the peak at −3.1 eV is observed, as shown by the displayed VB spectra (5) and (7). However, the most salient feature is the continuous growth of a new shoulder structure at −3.6 eV which is marked by a vertical line and becomes the dominant feature in the VB spectrum (10), representative for the high temperature oxidation steps (9)–(12) at 1100 K. The work function value as well as the peak structure of this spectrum are already widely similar to the reference VB spectrum (13) of bulk MoO_2, gained after the last oxidation step at 1250 K. The strong broad shoulder structure with a maximum intensity around −3.6 eV and the two peaks at −1.7 and −0.4 eV are in agreement with He I UP spectra of the conducting oxide MoO_2 reported in the literature [39,40].

Interestingly, the position of the maximum intensity of the strong broad shoulder structure varies for the He I MoO_2 spectra in the literature between −4.5 and −5.5 eV and is found for the MoO_2/Mo(1 1 2) system at the even lower value of −3.6 eV. This may indicate the presence of a heavily strained MoO_2 layer on the Mo(1 1 2) surface because Eyert et al. found in a theoretical calculation on the electronic structure of MoO_2 a strong shift of this mainly O_{2p} derived shoulder towards lower binding energies with an increase of the Mo–O bond distance [41]. Very important is also the low-binding energy region ($E_{Bin} > -2.5$ eV) of the VB spectrum. The double peak structure of mainly Mo_{4d} derived states is characteristic of the monoclinic MoO_2 crystal lattice of the growing oxide epilayer. As addressed in detail in the surface morphology study below, monoclinic MoO_2 shows a characteristic metal-metal dimerization along the *a*-axis of the lattice which is the result of a Peierls-type instability [41–43]. As a result of this distortion in the d^2-system MoO_2, chains of equidistant Mo atoms in the centers of edge-sharing oxygen octahedra break up in Mo–Mo dimers. The resulting dimers show a Mo–Mo bond length of 2.51 Å and are separated from each other by 3.11 Å along the *a*-axis. Certainly, this metal–metal pairing causes a simultaneous deformation of the octahedral oxygen coordination spheres so that the well-known octahedral crystal field splitting of the Mo_{4d} orbitals in a t_{2g}- and an e_g-band becomes modified. In particular, the reduction in symmetry results in a splitting of the occupied t_{2g}-band. Orbitals of former t_{2g} symmetry and directed towards next neighbour metal atoms form the metal–metal bonds, resulting in the creation of a bonding Mo-4d σ and an antibonding Mo-4d σ* band. Orbitals of former t_{2g} symmetry and directed perpendicular to the next neighbour metal atom direction are practically not involved in the metal–metal bonds and form a mostly non-bonding Mo-4d π band. Thus, the peaks at −1.5 and −0.4 eV in the low-binding energy region of the MoO_2 UP spectra (10) and (13) in Fig. 2 can be assigned to the bonding Mo-4d σ and non-bonding Mo-4d π states, respectively, directly reflecting the octahedra distortion in the monoclinic oxide structure.

3.3. STM study of the surface morphology

The main results of the STM study on the oxidation of the Mo(1 1 2) surface are summarized in Fig. 3. The visible drastic changes of the surface morphology during the exposure to oxygen are discussed in the following.

The STM study starts in Fig. 3 with the clean Mo(1 1 2) surface (0). The overview scan (0a) reveals the presence of terraces with a clearly elongated shape along the $[\bar{1}\,\bar{1}\,1]$ direction. This is due to a crystal miscut of about 0.14° towards the $[\bar{1}\,1\,0]$ direction. For both directions, line scans (not shown) across the terrace edges measure step heights of about 1.2 and 2.4 Å. According to the Mo(1 1 2) interlayer spacing derived by a dynamical LEED study [44], these values point to the presence of single- and double-layer steps on the surface. The high-resolution image (0b) is measured on a terrace and resolves a line structure along the $[\bar{1}\,\bar{1}\,1]$ direction. The corrugation between adjacent atoms along these lines is too small to deduce from our STM measurement the unit cell spacing of the Mo(1 1 2) surface along the $[\bar{1}\,\bar{1}\,1]$ direction. Along the $[\bar{1}\,1\,0]$ direction adjacent lines are found in the STM scan (0b) to be separated by 4.45 Å which equals the substrate spacing along this direction.

This is shown in the sketch of the Mo(1 1 2) crystal surface in Fig. 4a. The line structure detected in the STM scan (0b) corresponds to the close-packed atomic Mo rows of the first layer which build up the trough and row structure of the Mo(1 1 2) substrate. A rectangular surface unit cell results with an unit cell spacing of 2.73 and 4.45 Å along the $[\bar{1}\,\bar{1}\,1]$ and the $[\bar{1}\,1\,0]$ direction, respectively.

Surface disorder is detected by STM on the substrate terraces in form of point defects. Image (0b) in Fig. 3 shows that protrusions and depressions with an apparent height and depth of about 0.6 and 0.3 Å, respectively, are imaged and cover about 10% of the surface. As STM topographs are known to image oxygen impurities on metal surfaces as depressions, probably a mixture of oxygen adatoms as well as Mo point defects causes the detected depressions [45]. This is supported by the results of the XPS study which show at this state a

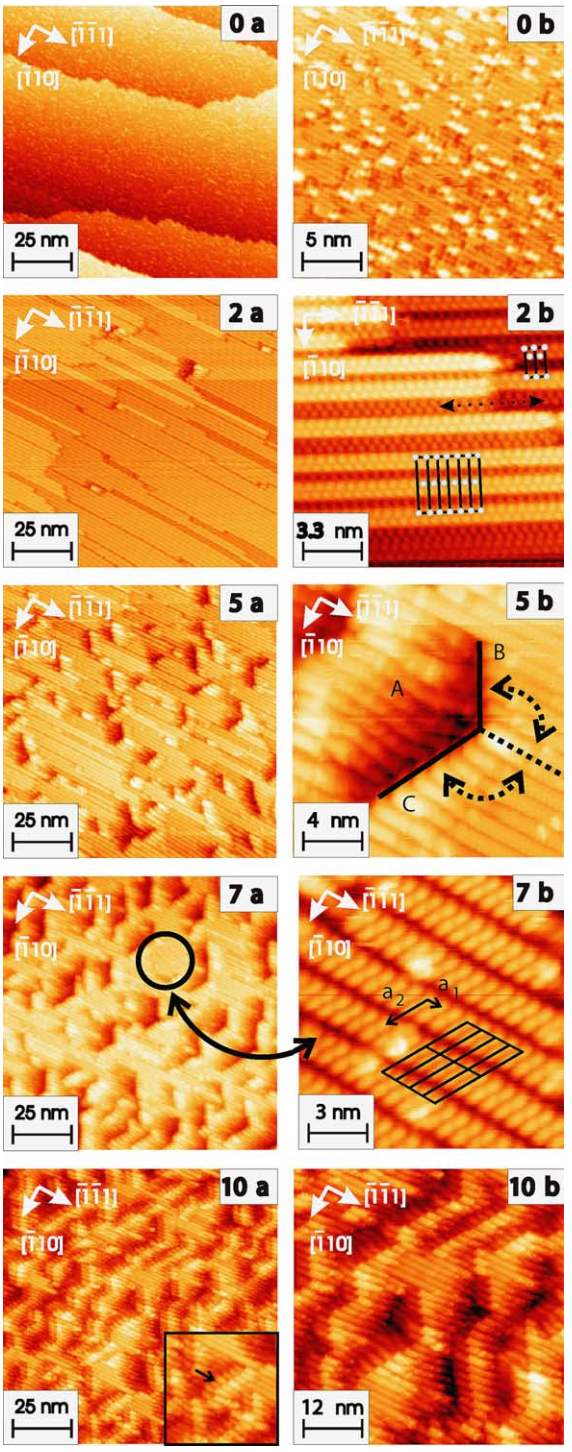

minor oxygen contamination. In contrast, no carbon impurities are measured by XPS so that most likely Mo adatoms are at the origin of the imaged protrusions.

The oxygen-induced p(2×3) reconstruction on the Mo(1 1 2) surface is prepared by applying the oxygen exposure steps (1) and (2). STM scans are shown in Fig. 3 in the images (2a) and (2b), supplementing the data presented by the authors in a previous publication on this reconstruction [25]. The overview scan (2a) reveals the well-evolved long-range order of this reconstruction by the presence of flat terraces with a very well-defined line structure along the $[\bar{1}\,\bar{1}\,1]$ direction. The distance between single stripes along the $[\bar{1}\,1\,0]$ direction is 13.35 Å so that the reconstruction induces a superstructure with three times the unit cell spacing of the clean Mo(1 1 2) surface. The scan (2b) with atomic resolution reveals that each of these stripes shows a fine structure. It is built up by two rows of protrusions running along the $[\bar{1}\,\bar{1}\,1]$ direction and being in a staggered arrangement with respect to each other. In each of these lines, adjacent protrusions show a distance of 5.46 Å along the $[\bar{1}\,\bar{1}\,1]$ azimuth which corresponds to twice the surface unit cell spacing of the unreconstructed substrate. In this way, a p(2×3) unit cell of the reconstructed surface phase results. The right upper corner of image (2b) shows a sketch of two such unit cells where gray dots are applied to mark the positions of the protrusions within the unit cells.

The structure model of the p(2×3) reconstruction is shown in Fig. 4b. This surface phase

Fig. 3. STM study of the oxidation of the Mo(1 1 2) surface. (0) Clean Mo(1 1 2) surface: (a) 100×100 nm^2, $U = -1$ V, $I = 4.5$ nA and (b) 20×20 nm^2, $U = -1$ V, $I = 4.5$ nA; (2) oxygen-induced p(2×3) reconstruction: (a) 100×100 nm^2, $U = -2.6$ V, $I = 0.27$ nA and (b) 12.5×12.5 nm^2, $U = -2.6$ V, $I = 0.1$ (nA); (5) after the 5th oxidation step: (a) 100×100 nm^2, $U = -1.31$ V, $I = 0.59$ nA and (b) 18×18 nm^2, $U = -1.31$ V, $I = 0.13$ (nA); (7) after the 7th oxidation step: (a) 100×100 nm^2, $U = -1.27$ V, $I = 0.71$ nA and (b) 12×12 nm^2, $U = -1.36$ V, $I = 4.65$ (nA); (10) after the 10th oxidation step: (a) 100×100 nm^2, $U = -1.27$ V, $I = 2.94$ nA and (b) 48×48 nm^2, $U = -1.27$ V, $I = 2.94$ (nA).

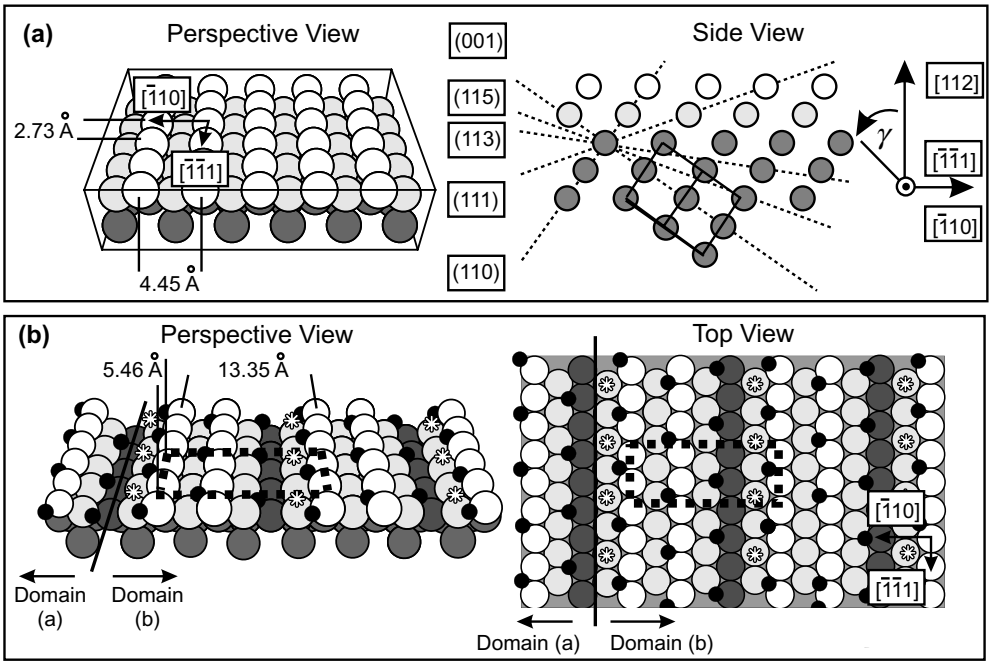

Fig. 4. Structure models with first, second and third layer Mo atoms sketched as white, gray and dark gray balls, respectively. (a) Perspective view: The trough and row structure of the clean Mo(1 1 2) surface is composed of the close-packed (1 1 1) rows of the Mo bcc lattice ($a = 3.15$ Å) which are in a staggered arrangement from layer to layer. The rectangular surface unit cell dimensions are indicated. Side view: the $(\bar{1}\,\bar{1}\,1)$ planes are not mirror planes of the Mo(1 1 2) surface. Passing from the [1 1 2] towards the $[\bar{1}\,\bar{1}\,1]([1\,1\,\bar{1}])$ direction, the surface normals of the lattice planes (dashed lines) [1 1 3]([1 1 1]), [1 1 5]([1 1 0]) and [0 0 1] are found at an angle γ of 10° (19.53°), 19.47° (54.7°) and 35.3°. Cubic bcc bulk unit cell is indicated by solid lines. (b) Reconstruction model of the p(2×3) O–Mo(1 1 2) system with oxygen atoms in quasi-threefold sites (black spheres) and on-top sites (asterisks). Perspective and top view: The p(2×3) unit cell is indicated by the dashed rectangular and the unit cell dimensions are shown. The black line depicts an antiphase domain boundary (see text for details).

is essentially a missing-row reconstruction [25]. Counting along the $[\bar{1}\,1\,0]$ direction, every third close-packed first layer Mo row is removed and this explains the observed three times spacing of the reconstructed unit cell spacing along this azimuthal direction. The origin of the doubled spacing of the superstructure along the $[\bar{1}\,\bar{1}\,1]$ direction is more complicated. Based on the results of the effective medium theory (EMT), the proposed structure model explains this fine structure as a direct consequence of the way oxygen adsorption generally takes place on transition metal surfaces [32,46]. As postulated by us on the basis of this theory [25] and meanwhile experimentally confirmed by Iwasawa et al. [23], the energetically most favored oxygen adsorption sites on the Mo(1 1 2) surface are the quasi-threefold coordination sites composed of two row atoms and one trough atom. Occupied sites of this type are sketched in the structure model in Fig. 4b by black dots. The tendency of oxygen atoms not to share low-coordinated Mo atoms in the adsorption process, at least not until the oxygen coverage is substantial, results in the occupation of only each second of these adsorption sites along a given close-packed Mo row. Furthermore, it makes a staggered arrangement of these occupied adsorption sites between two neighbouring Mo rows energetically more favorable. In this way, the adsorption of oxygen atoms in the quasi-threefold coordination sites results in the arrangement which is indicated by the black dots in Fig. 4b. As oxygen

on metal surfaces is imaged in STM scans as a pattern of depressions, the strong protrusions within each stripe can be traced back to the metal sites [47]. In consequence, the structure model describes each of these protrusions as being composed of two neighbouring first-layer Mo row atoms which appear unresolved in the STM images. In addition to oxygen adsorption in quasi-threefold coordination sites, oxygen is adsorbed in on-top positions to saturate undercoordinated second layer Mo row atoms. These oxygen atoms are depicted by asterisks in Fig. 4b and their presence is strongly supported by an infrared-reflection adsorption spectroscopy (IRAS) study [48].

Surface defects on reconstructed metal surfaces often show a very anisotropic behaviour [49,50]. This is also the case in the present study and, as outlined in [25], the long-range order along the $[\bar{1}\,1\,0]$ direction is highly disturbed by surface dislocations in form of antiphase domain boundaries. These boundaries run along the $[\bar{1}\,\bar{1}\,1]$ direction and such a dislocation is sketched in Fig. 4b in form of a black solid line. It separates the p(2×3) domains (a) and (b) which are displaced with respect to each other by one times the substrate spacing along the $[\bar{1}\,\bar{1}\,1]$ direction. Due to the resulting out-of phase relationship for scattering from different domains, low energy electron diffraction (LEED) studies identified the presence of these dislocations by the observed streakening behaviour of odd-order reflections. A periodic sequence of such antiphase domain boundaries with a spacing of 13.35 Å along the $[\bar{1}\,1\,0]$ direction will result in the presence of c(2×6) domains on the reconstructed surface. Image (2b) in Fig. 3 shows in the middle of the scan an example of such a c(2×6) domain with a sequence of c(2×6) unit cells depicted. However, these c(2×6) domains are rarely detected on the reconstructed surface and are in general much smaller than the p(2×3) domains. In contrast to this defect structure along the $[\bar{1}\,1\,0]$ direction, the long-range order along the $[\bar{1}\,\bar{1}\,1]$ direction is very well evolved. No surface dislocations are observed which break up the stripes. Only steps at terrace edges do so and such a step is marked in the topograph (2b) of Fig. 3 by the dashed arrow. Here, it can be noticed that the unidimensional rows in the stripes of two subsequent layers are in a staggered and not in an on-top configuration along the [1 1 2] direction.

The onset of the oxidation is detected by XPS and UPS during the third oxidation step and starts to transform the p(2×3) O–Mo(1 1 2) surface structure into a MoO_2 layer. The STM images (5a) and (5b) in Fig. 3 show the surface structure of a 15 ± 1.5 Å thick MoO_2 film and highlight the characteristic changes which the surface morphology undergoes during the early oxidation steps (3)–(5). It is clearly seen that the onset of the oxidation process is accompanied by a faceting of the reconstructed Mo(1 1 2) surface. This faceting process roughens the very flat reconstructed surface, in particular by the creation of holes (which appear as dark regions in the images). As can be deduced from the overview scan (5a), many of these holes exhibit a rather regular shape and the high resolution scan (5b) shows the three crystal faces *A*, *B* and *C* which usually form these facet structures. In case of the rather rough and irregular facet plane *A*, its surface normal is inclined away from the [1 1 2] towards the $[\bar{1}\,\bar{1}\,1]$ direction. STM line scans performed with a high loop gain deduce a mixture of inclination angles γ between 10° and 20°. In case of the planes *B* and *C*, the respective surface normals are found to be perpendicular to the [1 1 2] axis. Therefore, these planes can be classified as (1 1 2) zone planes. From the fact that the faces *B* and *C* enclose both an angle of $118 \pm 2°$ with respect to the $[\bar{1}\,\bar{1}\,1]$ direction, it is obvious that these faces are the boundaries of a twin structure within the oxide layer where the substrate $(\bar{1}\,1\,0)$ plane of the bcc lattice acts as the twinning plane.

An inspection of a stereographic plot of the bcc lattice supports the possibility of such a twin structure in the epitaxial oxide layer on Mo(1 1 2) [51]. It is seen that the (1 1 0) planes are mirror planes of bulk terminated (1 1 2) surfaces. However, it is important to note that this is not true for (1 1 1) planes. This point is illustrated in Fig. 4a in the side view sketch along the $[\bar{1}\,1\,0]$ direction of the bcc[1 1 2] substrate. The (1 1 1) planes are not mirror planes of the (1 1 2) substrate because the surface normals of the lattice planes between the [1 1 2] and $[\bar{1}\,\bar{1}\,1]$ direction are different from those

between the [1 1 2] and the [1 1 $\bar{1}$] direction. The side view sketch of Fig. 4a shows that only towards the [$\bar{1}$ $\bar{1}$ 1] direction surface normals of low index surface planes exist which exhibit inclination angles γ of 10° ((1 1 3) plane) and 19.42° ((1 1 5) plane). It is therefore reasonable to assume that the rough oxide facet planes *A*, imaged in scan (5b) of Fig. 3, grow on a mixture of (1 1 3) and (1 1 5) substrate planes. [1] Based on these results, a comparison with the stereographic plot of the bcc structure reveals furthermore that the orientations of the oxide faces *B* and *C* of scan (5b) in Fig. 3 agree within 4° with those of the low-index (1 1 2) zone planes (1 $\bar{3}$ 2) and ($\bar{3}$ $\bar{1}$ 2), respectively.

The progress in the oxidation process is detected in the STM study after the application of the 7th oxidation step. Comparing in Fig. 3 the overview STM scan (7a) with the corresponding image (5a) shows that further oxidation increases the number of holes in the surface and diminishes in that way the region of the oxide terraces oriented parallel to the [1 1 2] bcc Mo axis. One of these terrace regions is marked by a circle in scan (7a). This experimental finding suggests that this oxide surface is not an orientation of low surface energy of the MoO_2 lattice. Scans of atomic resolution can be performed on this face of MoO_2 during the oxidation steps (3)–(10) and a representative image is shown in picture (7b). The depicted surface unit cell is described by the basis vectors $\vec{a}_1 = 5.6 \pm 0.1$ Å and $\vec{a}_2 = 16.8 \pm 0.1$ Å which enclose an angle of $118 \pm 2°$.

To identify this face of MoO_2, the monoclinic MoO_2 bulk lattice structure with space group $P2_1/c$ (C^5_{2h}) is shown in Fig. 5a [42,52]. The lattice constants and the monoclinic angle amount to $\vec{a} =$ 5.6109 Å, $\vec{b} = 4.8562$ Å, $\vec{c} = 5.6285$ Å and $\beta =$ 120.95°, respectively. The MoO_2 unit cell length of the *a*-axis is very close to that of the *c*-axis so that both fit with the experimentally determined dimension of the surface unit cell vector $\vec{a}_1$ in the STM scan (7b). This ambiguity can be lifted by the following lattice considerations. On the one hand, the monoclinic MoO_2 lattice can be derived from the tetragonal rutile structure through a small distortion which, as sketched in Fig. 5a, results in a metal–metal dimerization along the crystallographic *a*-axis [41]. On the other hand, the presented structure model of the p(2×3) reconstruction suggests that (a) the characteristics of the oxygen adsorption behaviour on transition

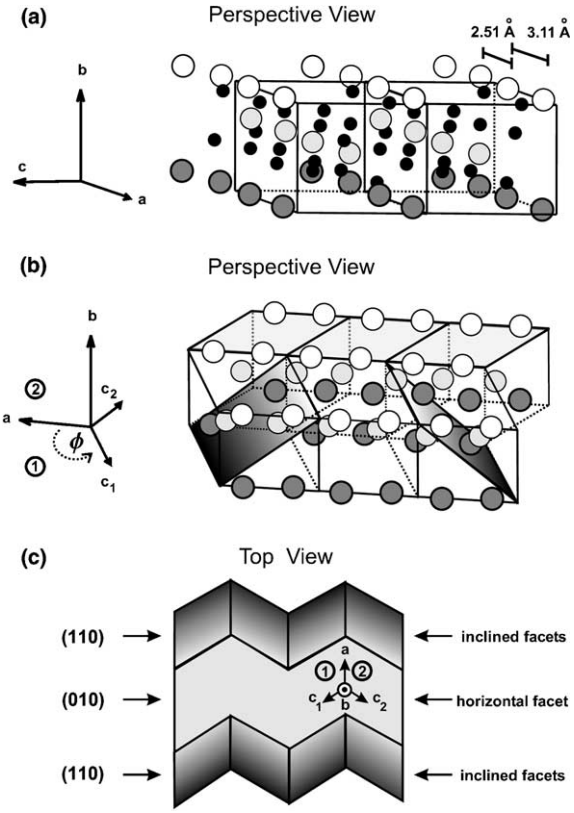

Fig. 5. (a) Two unit cells of the MoO_2 bulk structure with dimerized Mo atoms along the *a*-axis. The trough and row structure of the bulk terminated (0 1 0) MoO_2 face is formed by the first (white spheres) and second (light gray spheres) layer *a*-axes Mo rows. (b) Twin structure of the epitaxial (0 1 0)MoO_2 layer on Mo(1 1 2) with the (0 0 1) MoO_2 face as twinning plane. Three unit cells are shown for each of the twins (1) and (2). The oxygen sublattice is omitted for clarity. Twin (1) shows the two orientations of the (1 1 0) MoO_2 face (shaded gray planes) and twin (2) the orientation of the (0 1 0)MoO_2 face (gray planes). (c) Model of (0 1 0)MoO_2 layer (gray plane) with zigzag pattern of inclined (1 1 0) facets (shaded gray planes).

[1] Note that, as the surface normals of these low-index substrate planes are inclined away from the [1 1 2] towards the [$\bar{1}$ $\bar{1}$ 1] direction, this assignment fixes the orientation of the surface coordinate system depicted in the STM images.

metal surfaces directly initiate such a dimerization process of the Mo atoms in the close-packed atomic (1 1 1) rows of the Mo(1 1 2) substrate and that (b) these Mo–Mo dimers are at the origin of the protrusions which form in the STM images the unidimensional chain structures along the $[\bar{1}\,\bar{1}\,1]$ direction. As this p(2×3) phase precedes the MoO_2 formation, we believe that the oxide surface unit cell vector $\vec{a}_1$ with $[\bar{1}\,\bar{1}\,1]$ orientation in image (7b) can be identified with the dimerized *a*-axis of the MoO_2 lattice. This assignment is supported by the fact that the number of Mo atoms per MoO_2 unit cell is one along the *c*- and two along the *a*-axis so that only the *a*-axis of the MoO_2 lattice matches the number of Mo atoms within the close-packed Mo(1 1 1) rows of the bcc lattice. Based on this assignment, the oxide face imaged in scan (7b) of Fig. 3 can be found among the planes of the *a*-zone of the MoO_2 lattice, in particular among the low-index planes (0 0 1), (0 1 0) or (0 1 1). For the following reasons, this oxide face is probably correctly indexed as (0 1 0) MoO_2 face which exhibits a trough and row structure very similar to the Mo(1 1 2) surface (see Fig. 5a). Firstly, only the angle of the almost hexagonal (0 1 0) MoO_2 face fits well to the experimentally observed surface unit cell angle of $118 \pm 2°$ so that in particular the rectangular (0 0 1) surface can be ruled out. Secondly, the length of the surface unit cell vector $\vec{a}_2$ in the STM image (7b) is exactly equal to three times the *c*-axis of the MoO_2 lattice which builds up the surface unit cell vector of the MoO_2(0 1 0) face along this direction. In this way, the STM scan suggests the presence of a p(1×3) reconstructed MoO_2(0 1 0) surface. Thirdly, when moving along the surface normal from the surface into the bulk, the *a*-axis Mo rows of subsequent MoO_2(0 1 0) layers form a staggered arrangement, but an on-top configuration results in case of the MoO_2(0 1 1) planes. The latter arrangement is less probable because the bcc(1 1 1) Mo rows, from which the dimerized *a*-axes of the MoO_2 lattice result during the oxidation process, are in a staggered arrangement in case of the Mo(1 1 2) and the p(2×3) reconstructed surface. Experimental evidence is reported below that, also in case of the oxide film, the *a*-axes Mo rows of subsequent MoO_2 layers are in a staggered arrangement.

Identifying the surface regions of MoO_2 oriented parallel to the [1 1 2] Mo substrate direction as (0 1 0) MoO_2 planes renders the detected instability of the plane terrace surfaces during the oxidation process understandable. A comparison with the shape of MoO_2 single crystals reveals that in particular the close-packed (1 1 0) face is a stable low-energy surface orientation, but not the open trough and row (0 1 0) plane [53]. Hence, the faceting of the oxide layer during the oxidation process is probably driven by the tendency to transform the (0 1 0) faces into (1 1 0) surfaces. Fig. 5b shows the possible orientations of the MoO_2(1 1 0) crystal faces (shaded gray planes) for the epitaxial system (0 1 0)MoO_2/Mo(1 1 2). In the model, the MoO_2 *a*-axis coincides with the Mo(1 1 2) $[\bar{1}\,\bar{1}\,1]$ direction and it includes the observed twin structure of the oxide layer which is characterized by the twins (1) and (2) sharing a common (0 0 1) MoO_2 face. Certainly, the presence of twin (2) results in two additional (1 1 0) faces which, for reasons of clarity, are not depicted in the sketch. The surface normals of these four different (1 1 0) facets all enclose a polar angle of 45° with respect to the (0 1 0) MoO_2 normal, but differ by their azimuthal angles ϕ with respect to the *a*-axis of MoO_2. These azimuthal angles ϕ amount to 30.95° and 210.05° for the sketched (1 1 0) planes of twin (1) and values of 149.05° and 329.05° are derived for the not depicted (1 1 0) facets of twin (2). In consequence, the (1 1 0) facets of the different twins intersect at the twin boundaries. The top view sketch in Fig. 5c depicts this situation in form of the resulting zigzag patterns of inclined (1 1 0) facets which limit to the top and to the bottom the size of the horizontal (0 1 0) terraces (gray plane) of the twinned (0 1 0) MoO_2 layer.

The STM study reveals that the (0 1 0) MoO_2 layer, grown with its *a*-axes along the $[\bar{1}\,\bar{1}\,1]$ substrate direction, exhibits after faceting this characteristic zigzag surface morphology. According to the XPS results, the STM images (10a) and (10b) in Fig. 3 after application of the 10th oxidation step are obtained on a 28 ± 2.8 Å thick oxide film. The flat MoO_2(0 1 0) terrace regions almost completely vanished and the discussed zigzag pattern of inclined crystal faces is clearly visible. The azimuthal

orientation of these inclined facets agrees well with the presented structure model but it is difficult to extract the exact inclination angles of the rough facet planes from STM line scans. The STM images show that many of the facet planes exhibit rather a stepped than an atomically flat surface structure. An example of this step structure is given in the inset of figure (10a). It can be described by the formation of (0 1 0) (terrace: parallel to (1 1 2)) and (1 0 0) (step: perpendicular to (1 1 2)) MoO_2 microfacets. As indicated by the arrow, the Mo rows of different MoO_2 layers are found in a staggered arrangement in this step structure supporting the indexing of the horizontal oxide terrace planes as (0 1 0) MoO_2 faces. Probably, this step structure of the oxide layer presents a transition state in the process of (1 1 0) facet formation. These results of the STM study (formation of (1 1 0) facets; stepped facet surfaces) are supported by low energy electron diffraction (LEED) studies which will be published elsewhere [55].

Beyond the 10th oxidation step, it is noted for completeness that STM could not follow the further changes in the surface morphology. Strong roughening of the surface is detected which prevents the recording of STM images with detailed structural information.

4. Conclusion and outlook

A study of the complex oxidation behaviour of the Mo(1 1 2) surface using several surface science techniques is presented. XPS and UPS have been applied to follow in detail the changes of the electronic properties from the clean substrate to the MoO_2 oxide layer. A chemisorbed phase is found to precede the oxide formation which is astonishingly stable and passivates the Mo(1 1 2) surface against further oxidation during the initial oxidation process. STM reveals that this chemisorbed phase can be described as an oxygen-induced p(2×3) surface reconstruction of the missing-row type. With the help of the results of the effective medium theory, a structure model has been developed for this surface phase. It is characterized by the transformation of the former bcc(1 1 1) Mo rows in unidimensional Mo chains where the oxygen adsorption initiates a pairing of the Mo atoms to dimers. As this phase is identified as the precursor state of the MoO_2 formation, the bcc(1 1 1) Mo rows with paired Mo atoms are likely to become the *a*-axes of the MoO_2 lattice with its well-known Mo dimer structure. This idea is supported by high resolution STM scans which, by succeeding to resolve the surface unit cell, allow to describe the grown oxide surface as a (0 1 0) MoO_2 plane. However, a comparison with the shape of MoO_2 single crystals shows that the close (1 1 0), but not the open trough and row (0 1 0) MoO_2 surface is a low energy surface orientation. In consequence, despite the increase in surface area, the lowering of the total surface energy is the driving force in the observed formation of (1 1 0) facets in the (0 1 0) MoO_2 layer upon further oxidation. The resulting surface morphology is complicated by the presence of a twin structure in the oxide layer, as a result of the symmetry properties of the Mo(1 1 2) substrate.

The observed roughening of the surface after the formation of (1 1 0) facets makes it difficult to follow further changes in the surface morphology by STM. For this, and for undermining the presented structure models, a grazing incidence X-ray diffraction (GIXD) study of the surface morphology is under way at the European Synchrotron Radiation Facility (E.S.R.F.).

Acknowledgements

N.M. thanks the Studienstiftung des Deutschen Volkes for a fellowship. For financial support, we are grateful to a number of agencies: Deutsche Forschungsgemeinschaft (DFG), Bundesministerium für Bildung und Forschung (BMBF), Fonds der Chemischen Industrie, and NEDO (International Joint Research Grant on Photon and Electron Controlled Surface Processes).

References

[1] O.M. Braun, V.K. Medvedev, Sov. Phys. Usp. 32 (1989) 328.

[2] A.T. Loburets, A.G. Naumovets, Yu.S. Vedula, Surf. Sci. 399 (1998) 297.
[3] A. Kiejna, R.M. Nieminen, Phys. Rev. B 66 (2002) 085407.
[4] G. Godzik, T. Block, H. Pfnür, Phys. Rev. B 67 (2003) 125424.
[5] I. Yakovkin, Surf. Sci. 389 (1997) 48.
[6] C. Waldfried, D.N. McIlroy, J. Zhang, P.A. Dowben, G.A. Katrich, E.W. Plummer, Surf. Sci. 363 (1996) 296.
[7] T. McAvoy, J. Zhang, C. Waldfried, D.N. McIlroy, P.A. Dowben, O. Zeybeck, T. Bertrams, S.D. Barrett, Eur. Phys. J. B 14 (2000) 747.
[8] I.N. Yakovkin, J. Zhang, P.A. Dowben, Phys. Rev. B 63 (2001) 115408.
[9] H.-K. Jeong, T. Komesu, I.N. Yakovkin, P.A. Dowben, Surf. Sci. 494 (2001) L773.
[10] C. Waldfried, D.N. McIlroy, P.A. Dowben, J. Phys.: Condens. Matter 9 (1997) 10615.
[11] C. Waldfried, P.A. Dowben, O. Zeybek, T. Bertrams, S.D. Barrett, Thin Solid Films 338 (1999) 1.
[12] T. Schroeder, M. Adelt, B. Richter, M. Naschitzki, M. Bäumer, H.-J. Freund, Surf. Rev. Lett. 7 (1/2) (2000) 7.
[13] T. Schroeder, A. Hammoudeh, M. Pykavy, N. Magg, M. Adelt, M. Bäumer, H.-J. Freund, Solid-State Electron. 45 (8) (2001) 1471.
[14] T. Schroeder, J.B. Giorgi, M. Bäumer, H.-J. Freund, Phys. Rev. B 66 (2002) 165422.
[15] I.A. Toyashima, G.A. Somorjai, Catal. Rev. 19 (1979) 19.
[16] Y. Iwasawa, Adv. Catal. 35 (1987) 187.
[17] N. Floquet, O. Bertrand, J. Solid State Chem. 93 (1991) 96.
[18] K.T. Queeney, C.M. Friend, J. Chem. Phys. 109 (14) (1998) 6067.
[19] G. Mestl, T.K.K. Srinivasan, Catal. Rev.-Sci. Eng. 40 (4) (1998) 451.
[20] C.M. Friend, K.T. Queeney, D.A. Chen, Appl. Surf. Sci. 142 (1999) 99.
[21] K. Fukui, T. Aruga, Y. Iwasawa, Surf. Sci. 281 (1993) 241.
[22] T. Aruga, K. Tateno, K. Fukui, Y. Iwasawa, Surf. Sci. 324 (1995) 17.
[23] T. Sasaki, Y. Goto, R. Tero, K. Fukui, Y. Iwasawa, Surf. Sci. 502 (2002) 136.
[24] A.K. Santra, B.K. Min, D.W. Goodman, J. Vac. Sci. Technol. B 20 (5) (2002) 1897.
[25] T. Schroeder, J.B. Giorgi, N. Magg, A. Hammoudeh, M. Bäumer, H.-J. Freund, Phys. Rev. B 65 (2002) 115411.
[26] M. Frank, Thesis, Humboldt-Universität, Berlin, 2000.
[27] R.G. Musket, W. McLean, C.D. Colmenares, D.M. Makowiecki, W.J. Siekhaus, Appl. Surf. Sci. 10 (1982) 143.
[28] M.P. Seah, W.A. Dench, Surf. Interface Anal. 1 (1979) 2.
[29] B. Brox, I. Olefjord, Surf. Interface Anal. 13 (1988) 3.
[30] G.H. Smudde, P.C. Stair, Surf. Sci. 317 (1994) 65.
[31] K. Wandelt, Surf. Sci. Rep. 2 (1982) 1.
[32] J. Norskov, Rep. Prog. Phys. 53 (1990) 1253.
[33] S. Hufner, Photoelectron Spectroscopy, Springer-Verlag, 1994.
[34] J. Wood, Phys. Rev. 117 (1960) 714.
[35] Papaconstantopoulos, http://cst-www.nrl.navy.mil.
[36] V.L. Moruzzi, J.F. Janak, A.R. Williams, Calculated Electronic Properties of Metals, Pergamon Press, 1978.
[37] V.P. Belash, I.N. Klimova, V.I. Kormilets, V.Yu. Trubitsin, L.D. Finkelstein, Surf. Rev. Lett. 6 (3/4) (1999) 383.
[38] V.A. Bondzie, P. Kleban, D.J. Dwyer, Surf. Sci. 347 (1996) 319.
[39] T.A. Sasaki, T. Soga, H. Adachi, Phys. Stat. Sol. 113 (1982) 647.
[40] N. Beatham, A.F. Orchard, J. Electron Spectrosc. Relat. Phenom. 16 (1979) 77.
[41] V. Eyert, R. Horny, K.-H. Höck, S. Horn, J. Phys.: Condens. Matter 12 (2000) 4923.
[42] B.G. Brandt, A.C. Skapski, Acta Chim. Scand. 21 (1967) 661.
[43] J. Goodenough, Metallic oxides, in: H. Reiss (Ed.), Progress in Solid State Chemistry, Pergamon, Oxford, 1971.
[44] D. Kolthoff, H. Pfnür, A.G. Fedorus, V. Koval, A.G. Naumovets, Surf. Sci. 439 (1999) 224.
[45] J. Wintterlin, J. Trost, S. Renisch, R. Schuster, T. Zambelli, G. Ertl, Surf. Sci. 394 (1997) 159.
[46] F. Besenbacher, J.K. Norskov, Prog. Surf. Sci. 44 (1993) 5.
[47] C.J. Chen, Introduction to Scanning Tunneling Microscopy, Oxford University Press, 1993.
[48] T. Schroeder, Thesis, Humboldt-Universität, Berlin, 2001 (in English).
[49] J.K. Gimzewski, R. Berndt, R.R. Schlitter, Phys. Rev. B 45 (12) (1992) 6844.
[50] K.C. Prince, A. Morgante, D. Cvetko, F. Tommasini, Surf. Sci. 297 (1993) 235.
[51] B.D. Cullity, S.R. Stock, Elements of X-ray Diffraction, Prentice-Hall, 2001.
[52] D.B. Rogers, R.D. Shannon, A.W. Sleight, J.L. Gillson, Inorg. Chem. 8 (1969) 841.
[53] T. Sekiya, Mater. Res. Bull. 16 (1981) 841.
[54] G. Ertl, J. Kueppers, Low Energy Electron Diffraction and Surface Chemistry, 2nd ed., Verl. Chemie, Weinheim, 1985.
[55] T. Schroeder, C. Quiros, J. Zegenhagen, in press.